# Continuity between koniocellular layers of dorsal lateral geniculate and inferior pulvinar nuclei in common marmosets

Bing-Xing Huo*[1], Natalie Zeater*[2,3,4], Meng Kuan Lin[1], Yeonsook S. Takahashi[1], Mitsutoshi Hanada[1], Jaimi Nagashima[1], Brian C. Lee[5], Ulrike Grünert[2,3,4], Michael I. Miller[5], Marcello G.P. Rosa[6,7], Hideyuki Okano[1,8], Paul R. Martin[2,3,4], Partha P. Mitra[1,9]

[1] Laboratory for Marmoset Neural Architecture, RIKEN Center for Brain Science, Wako, Saitama, Japan
[2] Save Sight Institute and Department of Clinical Ophthalmology, The University of Sydney, Sydney, NSW 2000, Australia
[3]Australian Research Council Centre of Excellence for Integrative Brain Function, The University of Sydney, Sydney, NSW 2000, Australia
[4] School of Medical Sciences, The University of Sydney, Sydney, NSW 2000, Australia
[5] Department of Biomedical Engineering, Johns Hopkins University, Baltimore, MD, USA
[6] Department of Physiology and Biomedicine Research Institute, Monash University, Clayton, 3800 Victoria, Australia
[7] Australian Research Council Centre of Excellence for Integrative Brain Function, Monash University Node, Clayton, 3800 Victoria, Australia
[8] Department of Physiology, Keio University School of Medicine, Tokyo, Japan
[9] Cold Spring Harbor Laboratory, Cold Spring Harbor, NY 11724, USA

Abbreviated title: Continuous koniocellular layers of LGN and inferior pulvinar.

*These authors contributed equally to this work.

Corresponding author: Paul R. Martin paul.martin@sydney.edu.au

Funding Information: National Health & Medical Research Council (NHMRC) Project grant (number 1081441 to PRM, UG); the Australian Research Council Centre of Excellence for Integrative Brain Function (CE140100007 to UG and PRM); Brain Mapping of Integrated Neurotechnologies for Disease Studies (Brain/MINDS) from the Japan Agency for Medical Research and Development, AMED (JP17dm0207001); National Institutes of Health (NIH) Grant 5R01EB022899.

## Abstract

The koniocellular (K) layers of the dorsal lateral geniculate nucleus (LGN) and the calbindin-rich subdivisions of the inferior pulvinar nucleus are considered part of a thalamic matrix system which projects diffusely to superficial cortical layers. Activity in the matrix system is proposed to coordinate oscillatory activity in thalamocortical loops. Here we studied connections of LGN K layers and IPul in marmosets following injections of retrograde tracer, Fast Blue, in V1 and V2. We adopted a high-throughput neuro-histology pipeline, which enabled simultaneous brain region identification based on cytoarchitecture and fluorescent tracer localization. A computational routine was established to automatically cross-register fluorescent neurons to individual subdivisions of LGN and IPul. We found that both V1 and V2 receive inputs from K layers and IPul, whereas dominant outputs of magnocellular and

parvocellular layers of LGN were to V1 only. Retrograde labeled cells in lateral division of IPul merged seamlessly into the retrograde labeled cells in K layers. We hypothesize that the K layers and IPul form a contiguous functional subdivision of the dorsal thalamic matrix.

# Introduction

The primate thalamus is a collection of subcortical nuclei that integrate sensory signals and are reciprocally connected to the cortex. The thalamic nuclei are segregated based on histochemical and/or functional differences. Two thalamic nuclei are implicated in visual signal transmission to the cortex, the lateral geniculate nucleus (LGN) and pulvinar (Jones & Hendry, 1989; Saalmann & Kastner, 2011; Sherman & Guillery, 2001). On one hand, the LGN is seen as a primary relay of retinal signals to cortex while the visual parts of the pulvinar are seen as association areas, forming input-output loops with the visual cortices. However, parallel to the view that the LGN and pulvinar have distinct roles, both nuclei are also purported to play a role in synchronizing oscillatory activity of thalamocortical loops and modulate visual cortical activation (Saalmann & Kastner, 2011). It is difficult to determine if the modulation of visual cortex by the LGN and visual pulvinar are different. It is suggested that both nuclei contain cells that contribute to an underlying matrix of thalamic neurons responsible for synchronized oscillation in cortex ( Jones, 2001). Therefore, the question of whether the matrix cells of LGN and visual pulvinar constitute a single population of modulatory thalamic neurons arises.

The proclivity of some thalamic cells to be immunoreactive to calbindin is the main argument for their classification as “matrix” cells, while thalamic cells with parvalbumin immunoreactivity are classed as “core” cells (Jones, 2001). In the primate LGN, three cell classes are identifiable; parvocellular (P), magnocellular (M) and koniocellular (K). P and M cells constitute the principle laminae of the primate LGN, receive their driving input from midget and parasol retinal ganglion cells (respectively), project to layer IV of V1 and are immunoreactive for parvalbumin. In contrast, K cells are located between the primary LGN laminae, receive driving input from widefield retinal ganglion cells and the superior colliculus, have been shown to send projections to superficial layers of V1 as well as terminals in V2 and the middle temporal area (MT), and are immunoreactive for calbindin (Goodchild & Martin, 1998; J K Harting, Casagrande, & Weber, 1978; S. H. Hendry & Yoshioka, 1994; S. Hendry & Reid, 2000; Leventhal, Rodieck, & Dreher, 1981; Solomon, 2002; Szmajda, Grünert, & Martin, 2008). Furthermore, activity of K LGN cells is synchronized to V1 EEG, thus implicating these cells in the modulatory role of the LGN (Cheong, Tailby, Martin, Levitt, & Solomon, 2011).

The involvement of the pulvinar in visual signal transmission is less well understood than that of the LGN, however its importance in the maintenance of visual perception has been made clear through inactivation studies (Bender & Butter, 1987; Purushothaman, Marion, Li, & Casagrande, 2012; Wilke, Turchi, Smith, Mishkin, & Leopold, 2010). Two pulvinar subregions are involved in visual signal modulation: the lateral pulvinar and the inferior pulvinar. Both the lateral and inferior pulvinar makes reciprocal connections with V1, V2 and higher order visual cortices, project to superficial layers of cortex, and contain both calbindin and parvalbumin immunoreactive cells (L. A. Benevento & Rezak, 1976; Gutierrez, Cola, Seltzer, & Cusick, 2000; E. G. Jones & Hendry, 1989; Kaas & Lyon, 2007; Stichel, Singer, & Heizmann, 1988). However, important distinguishing features of inferior pulvinar connectivity are its dense, topographically organised inputs from superior colliculus (Louis A. Benevento & Standage, 1983; John K. Harting, Huerta, Frankfurter, Strominger, & Royce, 1980; Stepniewska, Qi, & Kaas, 2000) and evidence for input from widefield retinal ganglion cells (Kwan et al., 2018).

Due to their similarity in histochemical markers and anatomical organization with respect to their inputs and cortical outputs, we propose that the K cells of the LGN and cells in inferior

pulvinar make up a continuous population of thalamic cells primarily involved in regulating the synchronization of corticothalamic loops.

Here we describe anatomical evidence for functional continuity between the LGN K layers and inferior pulvinar by comparing their immunohistochemistry and connectivity with V1 and V2.

# Materials and Methods

**Immunohistochemistry for calbindin-positive cells**

Immunohistochemistry experiment was performed on a male adult common marmoset (*Calithrix jacchus*). Procedures were approved by the Institutional Animal Experimentation and Ethics Committee at the University of Sydney, and conform to the Society for Neuroscience and Australia National Health and Medical Research Council (NHMRC) policies on the use of animals in neuroscience research. Following up to 96 hours in which the marmoset was anaesthetized (intravenous sufentanil citrate infusion 6–30 $\mu g \cdot kg^{-1} \cdot h^{-1}$) for unrelated physiological experiments, the animal was euthanized (intravenous infusion of 300–600 mg $kg^{-1}$ sodium pentobarbitone) and perfused transcardially with 0.9% saline followed by 4% paraformaldehyde in 0.1 M phosphate buffer (PB, pH 7.4), then by 10% sucrose in PB. The brain was removed and immersed in 20% glycerol for 24–72 hr then coronally sectioned at 50 µm thickness on a freezing microtome. Sections were intially processed for visualisation of nissl substance. Sections were initially stained with NeuroTrace blue-fluorescent Nissl stain (1:100; Molecular Probes). Sections were then pre-incubated in PTD for 1 hour at room temperature. The tissue was subsequently incubated with a mixture of primary antibodies (rabbit anti Calbindin and mouse anti Cam Kinase II Abcam) for 2 days under slight agitation. Following this the sections were incubated with secondary antibodies (donkey anti-rabbit Alexa 488 and donkey anti-mouse Alexa 594) for 2 hours. It was not possible to identify any soma labelled for Cam Kinase however NeuroTrace blue and Calbindin were evident in all sections.

Table 1. Case information and injection sites for marmosets used in tracing study

| Animal ID | Sex | Age | Weight (g) | Target area | Injection site center | | |
|---|---|---|---|---|---|---|---|
| | | | | | ML (mm) | AP (mm) | Depth (mm) |
| 820 | F | 6y11mo | 400 | V1 | +1.8 | -8.05 | 0.95 |
| 822 | F | 7y | 355 | V2 | +6.6 | -6 | 0.7 |
| 919 | F | 8y8mo | 345 | V2 | +0.7 | -4.7 | 0.5 |
| 1144 | F | 10y3mo | 353 | V2 | +2.8 | -4.5 | 1.1 |
| 1146 | F | 7y1mo | 394 | V1 | +2.0 | -10 | 0.8 |
| 1148 | F | 4y3mo | 343 | V2 | +5.15 | -4 | 1.0 |

**Tracing study using the high-throughput neurohistology pipeline**

To study the cortical connections of LGN and IPul, we performed tracing study in six female common marmosets (*Callithrix jacchus*), acquired from the Japanese Central Institute for Experimental Animals and Japan National Institute for Basic Biology. Case information is shown in Table 1. All experimental procedures were approved by the Institutional Animal Care and Use Committee at RIKEN, and a field work license from Monash University and conducted in accordance with the Guidelines for Conducting Animal Experiments at RIKEN

Center for Brain Science and the Australian Code of Practice for the Care and Use of Animals for Scientific Purposes.

Retrograde tracer, Fast Blue (FB), was pressure injected in V1 in two cases and V2 in four cases. Each tracer was delivered using Nanoject II (Drummond, USA) with equal volume at depths of 1200µm, 800µm, and 400µm, controlled with Micro4 (WPI, USA), to fill the entire cortical column. Detailed surgical procedure for tracer injection was described previously(Alegro et al., 2017; Reser, Burman, Richardson, Spitzer, & Rosa, 2009; Reser et al., 2013). A summary of all injections is shown in Table 1.

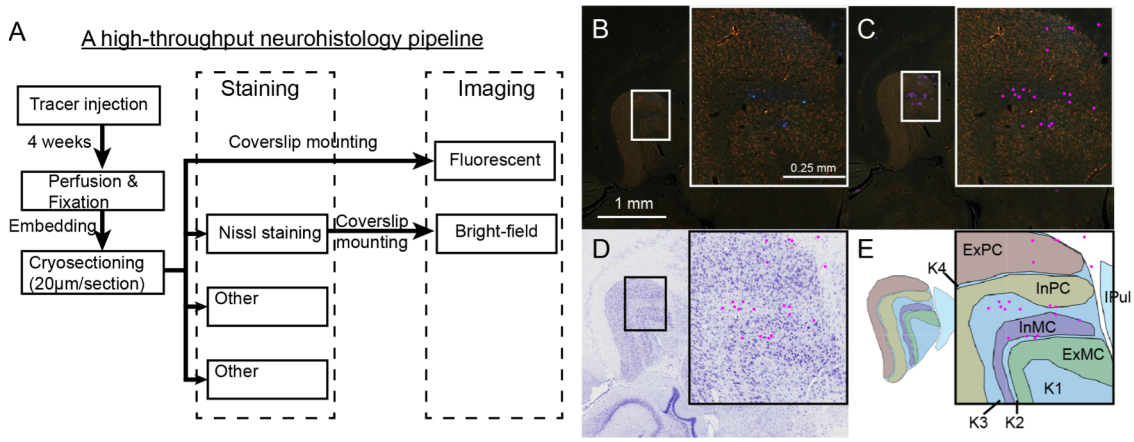


Fig. 1. **Experimental and computational workflow to study LGN and IPul connectivity with V1 and V2 in marmosets. A**. A schematic illustration of the high-throughput neurohistology pipeline for marmoset brain. Retrograde tracer, Fast Blue (FB), was injected in V1 or V2. Only Nissl sections and fluorescent sections were used in the current study. Details of this pipeline was described elsewhere (Mitra et al., 2016). **B-E**. A computational routine to identify the FB labeled cells in different brain regions. **B**. A part of the fluorescent image showing a coronal section of LGN. **C**. FB-labeled cells, some appeared bright while others were faint, were detected automatically and manually corrected (magenta dots). **D**. The fluorescent section was registered with the adjacent Nissl section. Detected cell coordinates were projected to the Nissl section (magenta dots). **E**. Subdivisions of LGN and pulvinar were manually segmented based on the Nissl section. Coordinates of the detected cells were translated into brain regions. ExPC: external parvocellular layer; InPC: internal parvocellular layer; InMC: internal magnocellular layer; ExMC: external magnocellular layer; K1-4: koniocellular layer 1-4.

A high-throughput neurohistology pipeline customized for marmosets was adopted to study the mesoscale connectivity(Mitra et al., 2016) (Fig. 1A). Briefly, after tracer injection and an incubation period of 4 weeks, the animal was euthanized and perfused. The brain was fixed with 4% paraformaldehyde, embedded in freezing agent (Neg-50$^{TM}$, Thermo Scientific 6505 Richard-Allan Scientific), and cryosectioned coronally using a tape-transfer method that was customized for marmoset brain. This method was originally developed for mouse brian(Pinskiy et al., 2015; 2013). Each brain section was 20µm thick. For every four consecutive sections, one was mounted the coverslip directly after dehydration, without any staining. The second section was processed with Nissl staining using an automatic Nissl staining system (Sakura Tissue-Tek Prisma). With the design of the custom tape-transfer method, different types of sections were processed in batches. The process of mounting coverslips was also automated using Sakura Tissue-Tek Glas, GLAS-g2-S0. The no-staining sections were scanned for fluorescent imaging using FITC/TX-RED/DAPI as excitation light filter; while the Nissl-stained sections were scanned with bright-field imaging. Therefore

every two consecutive fluorescent sections were separated by 80 μm; same with Nissl sections.

All brain sections were scanned in a high-throughput fashion in Nanozoomer 2.0 HT (Hamamatsu, Japan) and saved as 12-bit RGB images, with a resolution of 0.46 μm/pixel. The RAW images were processed in a high-performance computational infrastructure (Lin et al., 2016). Images of individual brain sections were isolated and compressed into JPEG2000 format for economic data storage and subsequent analyses.

**LGN and pulvinar segmentation**

A web portal (riken.marmoset.brainarchitecture.org) for image viewing and sharing was developed using Openlayer 3.0 image server and a custom image viewer. Within this portal, a web-based annotation tool was developed for brain region segmentation and annotation, as well as proofreading automatic cell detection results. For all brains in the current study, M and P layers of LGN and subdivisions of pulvinar were manually segmented based on Nissl sections using the web-based annotation tool by multiple annotators internationally, taking (Paxinos, Watson, Petrides, Rosa, & Tokuno, 2012) as the reference anatomical model (Fig. 1E). K layers of LGN were segmented by subtracting M and P layers from total area of LGN and divided into interlaminar regions. Volume of individual subdivisions were estimated with voxel size of $0.46 \times 0.46 \times 80\ \mu m^3$.

**Cell detection and brain region identification**

An automatic cell detection routine was developed to locate FB labeled cells in all brain sections. In short, a mask of the brain section was calculated to remove the glass slide background. A Mexican hat filter was applied to quench background and foreground noises. Color and intensity thresholds were applied to weakly filter the pixels. A series of morphological operations were performed to identify individual cells and clusters of cells. Clusters of cells were cut using an fast, unsupervised method (Pahariya et al., 2018). Coordinates of the cell centroids were recorded to represent individual cell location in the brain section. The results were uploaded to the web portal. Using the annotation tool, manual corrections were performed to remove false detections or add missing cells.

In order to identify the brain region where the FB labeled cells were detected, it was necessary to overlay the fluorescent section, which the cell coordinates were based on, with its adjacent Nissl section, where the brain region segmentation was based on. A computational routine was established to perform this process automatically for all brain sections, and illustrated in Fig. 1B-E. Briefly, rigid transformation between every two adjacent fluorescent and Nissl sections was performed using a custom algorithm based on simpleITK(Lowekamp, 2013; Yaniv, Lowekamp, Johnson, & Beare, 2017). The calculated transformation was applied to the detected and corrected cell coordinates, so that the cells were mapped onto the Nissl sections and the segmented brain regions. Based on individual regions, labeled cell numbers and the cell densities were estimated.

All data analyses algorithms were written in Matlab (R2017b, Mathworks, USA) and Python 2.7.13. Image processing, cell detection, and fluorescent-to-Nissl registration were performed on GNU Linux operating on Intel(R) Xeon(R) 24-core CPU workstation. Other data analyses, including volume and cell density estimation, were performed on a Macintosh computer (Apple, Inc.).

# Results

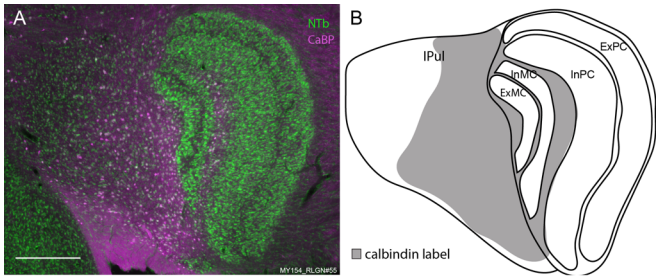


Fig. 2. **A** Photomicrograph of a coronal section through LGN and pulvinar. Soma stained for Nissl substance using NeuroTrace blue (NTb) are shown in green. Soma stained for Calbindin (CaBP) are shown in magenta. Scale bar is 500 µm. **B** Drawing outlining the boundaries of LGN laminae and inferior pulvinar (IPul) in A. The region with the densest calbindin labelling is shown in grey.

**Calbindin-positive cells continued seamlessly from K layers of LGN to IPul**

Calbindin staining revealed brightly labelled cells in both the LGN and IPul. In LGN, cells positive for calbindin were restricted to the K layers. The majority of calbindin positive cells where located in K1, K2 and K3.No clear cytoarchitectonic boundaries could be identified between LGN and IPul. The extension of calbindin-positive cells through the LGN K layers and IPul is demonstrated in Figure 2 whereby double labelling for Nissl substance (green) and calbindin (magenta) reveals the calbindin negative principle LGN laminae clearly and the calbindin positive cells K and IPul underlying the LGN laminae and forming a homogenous group.

**Both koniocellular (K) layers of LGN and IPul projected to V1 and V2**

To study the cortical connectivity of K layers of LGN and IPul, retrograde tracer, Fast Blue (FB), was injected in V1 in two cases and V2 in four cases. By employing the high-throughput neurohistology pipeline customized for marmosets(Mitra et al., 2016), we obtained consecutive coronal section images with Nissl staining and fluorescence.

For all brain sections, subdivisions of LGN and pulvinar were manually segmented using Nissl stained sections. We followed the nomenclature in Paxinos et al. (2012) (Paxinos et al., 2012) and were specifically interested in all layers of LGN and IPul. FB labeled cells were automatically detected and manually corrected in every fluorescent section, and cross-registered to its adjacent Nissl section for brain region identification (Fig. 1B). Cell density was estimated in the unit of number of cells per $mm^3$. In all cases, FB labeled cell bodies were found in K layers and IPul (Fig. 3A). Specifically, in both cases of V1 injection, all four K layers had FB labeled cells, with an average density of 605 ± 291 cells/$mm^3$ across all K layers. Among V2 injections, only K1 showed consistent, although sparse, labeling across all cases, with an average density of 28 ± 21 cells/$mm^3$. More neurons were labeled in K2 (171 ± 246 cells/$mm^3$) and K3 (207 ± 328 cells/$mm^3$) in 3 cases. Dense labeling in K4 was only observed in one case (379 cells/$mm^3$), which also had dense labeling in all other K layers (Fig. 3B). IPul showed consistent projections to both V1 and V2 in all cases, with cell density of 227 ± 176 cells/$mm^3$ for V1 injections and 354 ± 220 cells/$mm^3$ for V2 injections (Fig. 3).

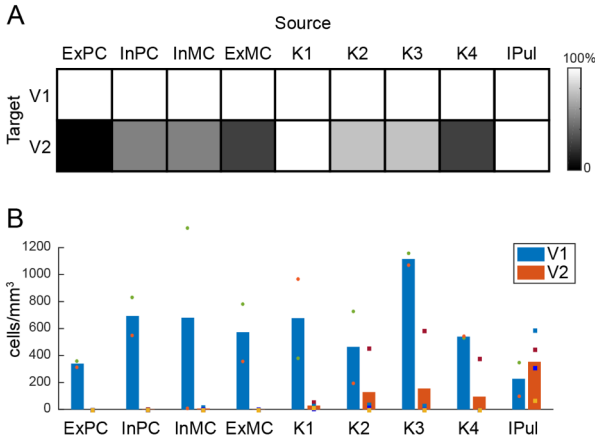


Fig. 3. **LGN and IPul connectivity with V1 and V2**. **A**. A connectivity matrix showing the probability that neurons from source regions (columns) were found projecting to the target regions (rows). The probability was estimated based on the existence of individual connections across all animals with the same injection site. That is, for connections showing a probability of 100% (white tiles), connection was found in all animals. Lower probability (darker tiles) indicates the connection was missing in some animals. **B**. Average cell density in individual brain regions detected for V1 (blue, N=2) or V2 (orange, N=4) injections. Cell density for each animal was plotted as dots for V1 injection, and squares for V2 injection.

**Primary layers of LGN predominantly projected to V1 only**

In marmosets, M and P layers were each subdivided into one external (ExMC, ExPC) and one internal layer (InMC, InPC). By examining the FB labeled cells in these individual layers, we found dense labeling in all layers in both cases of V1 injection, with an average density of 571 ± 163 cells/mm$^3$. However, in the case of V2 injection, FB labeled cells were very sparse or nonexistent in M and P layers of LGN (Fig. 3A). No FB labeled cells were detected in ExPC in any case. In InPC and InMC, two cases showed FB labeling, with average densities of 4 cells/mm$^3$ for InPC and 14 cells/mm$^3$ for InMC. Only one case had FB labeling in ExMC layer, with a density of 5 cells/mm$^3$ (Fig. 3B).

**Retrograde labeled cells continued from IPul to K layers of LGN**

For both V1 and V2 injections, FB labeled cells were detected more laterally from posterior to anterior sections. One example with V2 injection is shown in Fig. 4A. Dense labeling of neurons were detected in lateral part of IPul and lateral pulvinar in more posterior coronal sections (Fig. 4A,a). In the consecutive fluorescent sections toward the brain anterior, the labeled neurons were detected in more lateral part of IPul (Fig. 4A,a-d), until they were detected in K layers of LGN (Fig. 4A,d). In more anterior sections, the labeled cells were also detected more laterally in K layers (Fig. 4A,d-h), while the cell density went down. By surveying all cases, with both V1 and V2 injections, we found the trend that from the posterior to anterior, FB labeled cells continued towards caudolateral brain regions, that is, in the order of IPul, K1, K2 and K3. In more caudolateral side of K4, labeled cells were detected in the case of V1 injection in more anterior sections. K4 labeling was rare in the case of V2 injection. Only one case showed sparse FB labeling in K4 (Fig. 4B). To quantify this transition from IPul to K layers, we matched the first section that IPul appeared, from anterior to posterior direction, as the baseline across all cases. We restricted the anterior-posterior range within -0.4 mm to +0.88 mm relative to this baseline section and calculated the average cell numbers per section within either IPul or K layers. We found that for V1 injection, there were 7 cells/section in IPul compared with 17 cells/section in K layers; for V2 injection, there were 23 cells/section in IPul compared with only 1 cell/section in K layers.

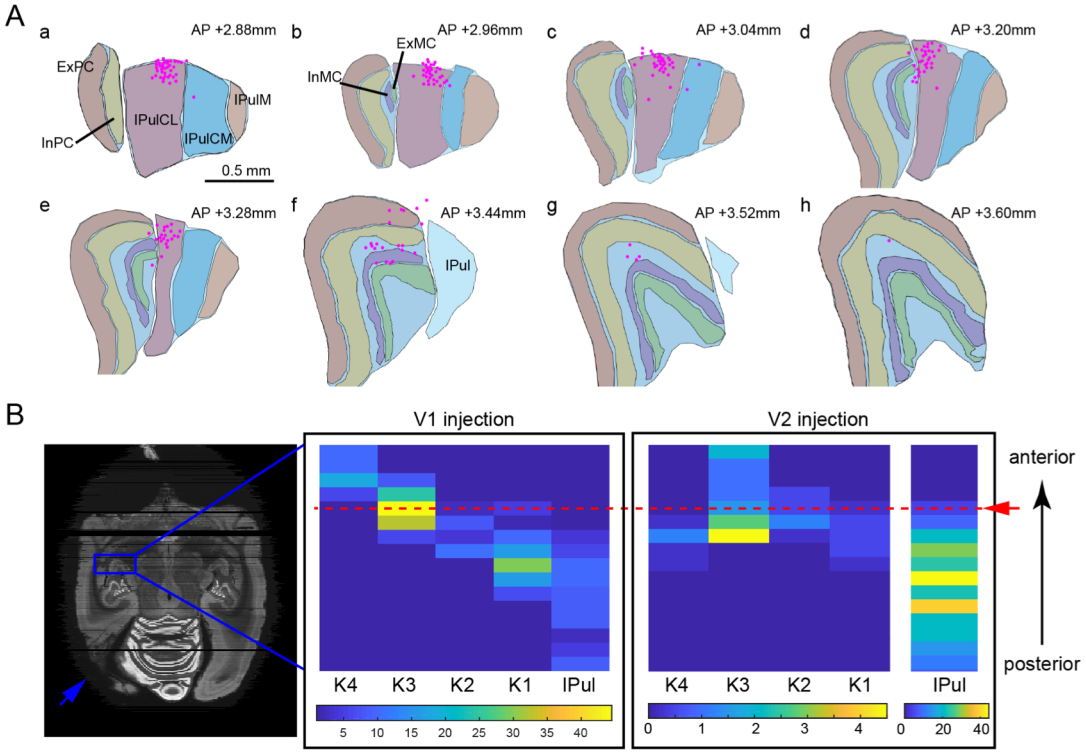


Fig. 4. **FB labeled cells continued seamlessly from IPul to K layers of LGN**. **A**. Reconstructed outlines of LGN and pulvinar subdivisions for case 822 from posterior (a) to anterior (g) direction. Magenta dots show positions of labeled cells. IPulCL: caudolateral part of IPul; IPulCM: caudomedial part of IPul; IPulM: medial part of IPul. **B**. *Left*: a volumetric reconstruction of the brain from coronal sections, in transverse view. A limited region (blue box) of the brain was isolated for each animal, and the number of cells detected in individual brain regions was counted for every coronal sections within this region. The injection site at V1 located in the very posterior part of the brain (blue arrow). *Right*: Two sets of matrices showing the number of cells in different regions for every coronal section after V1 or V2 injection. Within each matrix, each tile represented the cell number in a certain brain region at one coronal section. The most posterior section was shown at the bottom while the most anterior section was at the top. Sections from different animals were lined up by matching the first section that IPul appeared (red dash line), when examining from anterior-to-posterior direction. The intensity of the tile corresponded to the cell numbers averaged across all animals for each injection location. On the bottom showed the correspondence between image intensity and cell numbers.

# Discussion

The main findings of this study were: 1) the calbindin positive cells in IPul and LGN formed a cytoarchitechtonically continuous population of cells. 2) Both LGN K layers and IPul send projections to V1 and V2, compared to the P and M LGN layers which only project to V1. 3) The thalamic projection to V1 and V2 had a lateral to medial organization that crossed the borders between the LGN K layers and the lateral part of IPul (IPulL). These results showed that the K layers of LGN and IPul are anatomically continuous, and with similar cortical projection patterns. Below we consider the significance of these results

The abundance of calbindin-positive neurons in IPul and LGN K cells of primates has been well documented (Cusick, Scripter, Darensbourg, & Weber, 1993; Goodchild & Martin, 1998; Johnson & Casagrande, 1995; E. G. Jones & Hendry, 1989a; Edward G Jones, 2001). In an assessment of the distribution of calcium binding proteins throughout the thalamus, Jones (1998) made mention of the extension of calbindin positive LGN cells into IPul in

macaque monkeys. In the current study, we have demonstrated this anatomical continuity between IPul and the K layers of marmoset LGN via both histochemical staining for calbindin and tracer studies between these thalamic nuclei and early visual cortex. Several studies corroborate our observations of continuity between the LGN K cells and IPul. Kwan et al. (2018) demonstrated that retinal ganglion cells projecting to a sub-division of IPul in the marmoset had widefield morphologies including broad thorny, recursive bistratified, narrow thorny and large bistratified cells. Similar morphologies of retinal ganglion cells have been observed to project to the K layers of marmoset LGN (Masri, Percival, Koizumi, Martin, & Grünert, 2017; Percival et al., 2014; Szmajda et al., 2008). One retinal ganglion cell type not observed to project to IPul was the small bistratified cell (SBC). SBCs carry the short wavelength cone signal (blue colour signal) to the brain and are known to also project to the LGN K layers (Szmajda, Grünert, & Martin, 2008; Tailby, Szmajda, Buzás, Lee, & Martin, 2008). This may reflect the dual role of the cells in the thalamus which can either be involved in the relay of sensory signals from the periphery to cortex (those K cells with SBS input) or in the modulation and synchronization of cortical activity (K cells receiving wide-field cell input).

The thalamic matrix cells, which are calbindin-immunoreactive, were implicated in synchronizing the thalamocortical activity(Jones, 2001). In LGN, these are the K cells, as a part of the ventral stream pathway from retina to the visual cortex. Inferior pulvinar, also abundant with calbindin-positive cells, plays a similar role in connecting retina and visual cortex in the ventral stream(Kwan et al., 2018; Rezak & Benevento, 1979). With the proximity and continuity between these calbindin-positive K cells and IPul cells, there is a possibility they belong to the same population. Further investigation of the specific retinal connections will be needed to confirm this possibility.

# References

Alegro, M., Theofilas, P., Nguy, A., Castruita, P. A., Seeley, W., Heinsen, H., et al. (2017). Automating cell detection and classification in human brain fluorescent microscopy images using dictionary learning and sparse coding. *Journal of Neuroscience Methods*, *282*, 20–33. http://doi.org/10.1016/j.jneumeth.2017.03.002

Bender, D. B., & Butter, C. M. (1987). Comparison of the effects of superior colliculus and pulvinar lesions on visual search and tachistoscopic pattern discrimination in monkeys. *Experimental Brain Research*, *69*(1), 140–154. https://doi.org/10.1007/BF00247037

Benevento, L. A., & Rezak, M. (1976). The cortical projections of the inferior pulvinar and adjacent lateral pulvinar in the rhesus monkey (macaca mulatta): An autoradiographic study. *Brain Research*. https://doi.org/10.1016/0006-8993(76)90160-8

Benevento, L. A., & Standage, G. P. (1983). The organization of projections of the retinorecipient and nonretinorecipient nuclei of the pretectal complex and layers of the superior colliculus to the lateral pulvinar and medial pulvinar in the macaque monkey. *The Journal of Comparative Neurology*, *217*(3), 307–336. https://doi.org/10.1002/cne.902170307

Casagrande, V. A., & Kaas, J. H. (1994). The Afferent, Intrinsic, and Efferent Connections of Primary Visual Cortex in Primates. In *Primary Visual Cortex in Primates* (Vol. 10, pp. 201–259). Boston, MA: Springer, Boston, MA. http://doi.org/10.1007/978-1-4757-9628-5_5

Casagrande, V., Yazar, F., Jones, K., & Ding, Y. (2007). The Morphology of the Koniocellular Axon Pathway in the Macaque Monkey. *Cerebral Cortex*, *17*(10), 2334–2345. http://doi.org/10.1093/cercor/bhl142

Cheong, K. S., Tailby, C., Martin, P. R., Levitt, J. B., & Solomon, S. G. (2011). Slow intrinsic rhythm in the koniocellular visual pathway. *Proceedings of the National Academy of Sciences of the United States of America*, *108*(35), 14659–14663. https://doi.org/10.1073/pnas.1108004108

Cusick, C. G., Scripter, J. L., Darensbourg, J. G., & Weber, J. T. (1993). Chemoarchitectonic subdivisions of the visual pulvinar in monkeys and their connectional relations with the middle temporal and rostral dorsolateral visual areas, MT and DLr. *Journal of Comparative Neurology*, *336*(1), 1–30. http://doi.org/10.1002/cne.903360102

Goodchild, A. K., & Martin, P. R. (1998). The distribution of calcium-binding proteins in the lateral geniculate nucleus and visual cortex of a New World monkey, the marmoset, Callithrix jacchus. *Vis Neurosci*, *15*(4), 625–642.

Gutierrez, C., Cola, M. G., Seltzer, B., & Cusick, C. (2000). Neurochemical and connectional organization of the dorsal pulvinar complex in monkeys. *The Journal of Comparative Neurology*, *419*(1), 61–86. https://doi.org/10.1002/(SICI)1096-9861(20000327)419:1<61::AID-CNE4>3.0.CO;2-I

Harting, J. K., Casagrande, V. A., & Weber, J. T. (1978). The projection of the primate superior colliculus upon the dorsal lateral geniculate nucleus: autoradiographic demonstration of interlaminar distribution of tectogeniculate axons. *Brain Research*, *150*, 593–599.

Harting, J. K., Huerta, M. F., Frankfurter, A. J., Strominger, N. L., & Royce, G. J. (1980). Ascending pathways from the monkey superior colliculus: An autoradiographic analysis. *The Journal of Comparative Neurology*, *192*(4), 853–882. https://doi.org/10.1002/cne.901920414

Hendry, S. H., & Yoshioka, T. (1994). A neurochemically distinct third channel in the macaque dorsal lateral geniculate nucleus. *Science (New York, N.Y.)*, *264*(5158), 575–577.

Hendry, S., & Reid, C. (2000). The Koniocellular Pathway in Primate Vision. *Annu. Rev. Neurosci.*, *23*, 127–153. https://doi.org/10.1146/annurev.physiol.66.032102.111604

Johnson, J. K., & Casagrande, V. A. (1995). Distribution of calcium-binding proteins within the parallel visual pathways of a primate (Galago crassicaudatus). *The Journal of Comparative Neurology*, *356*(2), 238–260. https://doi.org/10.1002/cne.903560208

Jones, E. G. (2001). The thalamic matrix and thalamocortical synchrony. *Trends in Neurosciences*, *24*(10), 595–601. https://doi.org/10.1016/S0166-2236(00)01922-6

Jones, E. G., & Hendry, S. H. C. (1989). Differential Calcium Binding Protein Immunoreactivity Distinguishes Classes of Relay Neurons in Monkey Thalamic Nuclei. *The European Journal of Neuroscience*, *1*(3), 222–246. https://doi.org/10.1111/j.1460-9568.1989.tb00791.x

Kaas, J. H., & Lyon, D. C. (2007). Pulvinar contributions to the dorsal and ventral streams of visual processing in primates. *Brain Research Reviews*, *55*(2), 285–296. http://doi.org/10.1016/j.brainresrev.2007.02.008

Kwan, W. C., Mundinano, I.-C., de Souza, M. J., Lee, S. C. S., Martin, P. R., Grünert, U., & Bourne, J. A. (2018). Unravelling the subcortical and retinal circuitry of the primate inferior pulvinar. *Journal of Comparative Neurology*. https://doi.org/10.1002/cne.24387

Leventhal, A. G., Rodieck, R. W., & Dreher, B. (1981). Retinal ganglion cell classes in the Old World monkey: morphology and central projections. *Science*, *213*(4512), 1139–1142. https://doi.org/10.1126/science.7268423

Lin, M. K., Takahashi, Y. S., Weber, K., Hossain, K., Huo, B., Tolpygo, A., et al. (2016, November 14). Computational infrastructure to enable whole-brain mesoscale circuit mapping for Marmoset. *Society for Neuroscience*. San Diego.

Lowekamp, B. C. (2013). The Design of SimpleITK, 1–14. http://doi.org/10.3389/fninf.2013.00045/abstract

Masri, R. A., Percival, K. A., Koizumi, A., Martin, P. R., & Grünert, U. (2017). Survey of retinal ganglion cell morphology in marmoset. *Journal of Comparative Neurology*. https://doi.org/10.1002/cne.24157

Mitra, P. P., Takahashi, Y. S., Weber, K., Lin, M. K., Hossain, K., Huo, B., et al. (2016). A High-Throughput Neurohistological Pipeline for Whole-Brain Mesoscale Circuit Mapping for Marmoset. Presented at the Society for Neuroscience, San Diego.

Pahariya, G., Das, S., Jayakumar, J., Bannerjee, S., Vangala, V., Ram, K., & Mitra, P. P. (2018). High precision automated detection of labeled nuclei in terabyte-scale whole-brain volumetric image data of mouse. *bioRxiv*, 252247. http://doi.org/10.1101/252247

Paxinos, G., Watson, C., Petrides, M., Rosa, M., & Tokuno, H. (2012). The marmoset brain in stereotaxic coordinates. http://doi.org/10.1016/j.brainresbull.2013.01.009

Percival, K. A., Koizumi, A., Masri, R. A., Buzás, P., Martin, P. R., & Grünert, U. (2014). Identification of a pathway from the retina to koniocellular layer K1 in the lateral geniculate nucleus of marmoset. *The Journal of Neuroscience*, *34*(11), 3821–3825. https://doi.org/10.1523/JNEUROSCI.4491-13.2014

Pinskiy, V., Jones, J., Tolpygo, A. S., Franciotti, N., Weber, K., & Mitra, P. P. (2015). High-Throughput Method of Whole-Brain Sectioning, Using the Tape-Transfer Technique. *Plos One*, *10*(7), e0102363. http://doi.org/10.1371/journal.pone.0102363

Pinskiy, V., Tolpygo, A. S., Jones, J., Weber, K., Franciotti, N., & Mitra, P. P. (2013). A low-cost technique to cryo-protect and freeze rodent brains, precisely aligned to stereotaxic coordinates for whole-brain cryosectioning. *Journal of Neuroscience Methods*, *218*(2), 206–213. http://doi.org/10.1016/j.jneumeth.2013.03.004

Purushothaman, G., Marion, R., Li, K., & Casagrande, V. a. (2012). Gating and control of primary visual cortex by pulvinar. *Nature Neuroscience*, *15*(6), 905–912. https://doi.org/10.1038/nn.3106

Reser, D. H., Burman, K. J., Richardson, K. E., Spitzer, M. W., & Rosa, M. G. P. (2009). Connections of the marmoset rostrotemporal auditory area: express pathways for analysis of affective content in hearing. *European Journal of Neuroscience*, *30*(4), 578–592. http://doi.org/10.1111/j.1460-9568.2009.06846.x

Reser, D. H., Burman, K. J., Yu, H.-H., Chaplin, T. A., Richardson, K. E., Worthy, K. H., & Rosa, M. G. P. (2013). Contrasting patterns of cortical input to architectural subdivisions of the area 8 complex: a retrograde tracing study in marmoset monkeys. *Cerebral Cortex (New York, N.Y. : 1991)*, *23*(8), 1901–1922. http://doi.org/10.1093/cercor/bhs177

Rezak, M., & Benevento, L. A. (1979). A comparison of the organization of the projections of the dorsal lateral geniculate nucleus, the inferior pulvinar and adjacent lateral pulvinar to primary visual cortex (area 17) in the macaque monkey. *Brain Research*, *167*(1), 19–40. http://doi.org/10.1016/0006-8993(79)90260-9

Saalmann, Y. B., & Kastner, S. (2011). Cognitive and perceptual functions of the visual thalamus. *Neuron*, *71*(2), 209–23. https://doi.org/10.1016/j.neuron.2011.06.027

Sherman, S. ., & Guillery, R. W. (2001). *Exploring the Thalamus*. *Exploring the Thalamus*. Elsevier. https://doi.org/10.1016/B978-012305460-9/50016-2

Solomon, S. G. (2002). Striate cortex in dichromatic and trichromatic marmosets: Neurochemical compartmentalization and geniculate input. *The Journal of Comparative Neurology*, *450*(4), 366–381. https://doi.org/10.1002/cne.10327

Stepniewska, I., Qi, H. X., & Kaas, J. H. (2000). Projections Of The Superior Colliculus To Subdivisions Of The Inferior Pulvinar In New-World And Old-World Monkeys. *Visual Neuroscience*, *17*(4), 529–549.

Stichel, C. C., Singer, W., & Heizmann, C. W. (1988). Light and electron microscopic immunocytochemical localization of parvalbumin in the dorsal lateral geniculate nucleus of the cat: evidence for coexistence with GABA. *The Journal of Comparative Neurology*, *268*(1), 29–37. https://doi.org/10.1002/cne.902680104

Szmajda, B. A., Grünert, U., & Martin, P. R. (2008). Retinal ganglion cell inputs to the koniocellular pathway. *The Journal of Comparative Neurology*, *510*(3), 251–268. https://doi.org/10.1002/cne.21783

Tailby, C., Szmajda, B. A., Buzás, P., Lee, B. B., & Martin, P. R. (2008). Transmission of blue (S) cone signals through the primate lateral geniculate nucleus. *The Journal of Physiology*, *586*(24), 5947–5967. https://doi.org/10.1113/jphysiol.2008.161893

Wilke, M., Turchi, J., Smith, K., Mishkin, M., & Leopold, D. A. (2010). Pulvinar inactivation disrupts selection of movement plans. *The Journal of Neuroscience*, *30*(25), 8650–8659. https://doi.org/10.1523/jneurosci.0953-10.2010

Yaniv, Z., Lowekamp, B. C., Johnson, H. J., & Beare, R. (2017). SimpleITK Image-Analysis Notebooks: a Collaborative Environment for Education and Reproducible Research. *Journal of Digital Imaging*, *490*, 1–14. http://doi.org/10.1007/s10278-017-0037-8